Inner strut morphology is the key parameter in producing highly porous and mechanically stable poly(-caprolactone) scaffolds via selective laser sintering

Inner strut morphology is the key parameter in producing highly porous and mechanically stable poly(ε-caprolactone) scaffolds via selective laser sintering

Tortorici Martina [a,g], *Gayer Christoph* [b], *Torchio Alessandro* [c,d], *Cho Simone* [a], *Schleifenbaum Johannes Henrich* [b,e], *Petersen Ansgar* [a,f]

[a] Julius Wolff Institut, Charité - Universitaetsmedizin Berlin, Augustenburger Platz 1, 13353 Berlin, Germany[b] Fraunhofer Institute for Laser Technology ILT, Steinbachstr. 15, 52074 Aachen, Germany

[c] Politecnico di Torino, Department of Mechanical and Aerospace Engineering, Corso Duca degli Abruzzi 24, 10129, Turin, Italy

[d] Università degli Studi di Torino, Department of Surgical Sciences, Corso Dogliotti 14, 10126, Turin, Italy

[e] RWTH Aachen University - Digital Additive Production DAP, Steinbachstrasse 15, 52074 Aachen, Germany

[f] BIH Center for Regenerative Therapies (BCRT), Charité - Universitaetsmedizin Berlin, Augustenburger Platz 1, 13353 Berlin, Germany

[g] Berlin-Brandenburg School for Regenerative Therapies, Charité - Universitaetsmedizin Berlin, Augustenburger Platz 1, 13353 Berlin, Germany

Abstract

Selective laser sintering (SLS) is an established method to produce dimensionally accurate scaffolds for tissue engineering (TE) applications, especially in bone. In this context, the FDA-approved, biodegradable polymer poly(ε-caprolactone) (PCL) has been suggested as a suitable scaffold material. However, PCL scaffold mechanical stability – an attribute of particular importance in the field of bone TE – was not considered as a primary target for SLS process parameters optimization so far. Here, we investigated the influence of SLS process parameters on the sintered scaffolds with the aim of producing highly porous (> 70% porosity) PCL scaffolds with sub-mm geometrical features for bone TE. Specifically, we studied the influence of laser power, beam compensation and laser beam diameter on the dimensional accuracy and mechanical stiffness of the produced PCL scaffolds. We found that the ratio between the diameter of the molten cross-section within scaffold struts and the outer strut diameter (including partially sintered particles) depended on the SLS process parameters. By maximizing this ratio, the mechanical stability could be optimized. The comparison with *in silico* predictions of scaffold mechanical stiffness revealed that the diameter of the molten cross-section within struts and not the strut diameter controlled the mechanical behaviour of the scaffold. These observations should be considered when evaluating the quality of the sintering

process based on dimensional accuracy, especially for features < 1 mm. Based on these findings, we suggested an approach to evaluate the sintering outcome and to define SLS process parameters that enable the production of highly porous scaffolds that are both dimensionally accurate and mechanically stable. Moreover, the cytocompatibility of PCL scaffolds was evaluated by elution tests with primary human mesenchymal stromal cells. No evidence of cytotoxicity was found in any of the investigated scaffolds, confirming the suitability of SLS as production technique of PCL scaffolds for bone TE over a wide range of SLS process parameters.

Keywords

Selective laser sintering; poly(ε-caprolactone); tissue engineering; bone; scaffold; cytocompatibility.

1. Introduction

Selective laser sintering (SLS) is an additive manufacturing (AM) technique that uses a CO_2 laser beam to fuse particles and build three-dimensional (3D) objects in a layer-by-layer fashion [1]. Due to its features, such as the possibility to reproduce complex 3D shapes without the need of an additional support material [1,2] nor the use of potentially toxic binders [2], the technique has gained attention for scaffold production in the field of tissue engineering (TE), whose aim is the restoration, maintenance or improvement of living tissue functions [3]. Moreover, many suitable TE materials can be processed by SLS [4,5], including poly(ε-caprolactone) (PCL), which is an FDA-approved biodegradable polymer [6]. Pure PCL scaffolds produced by SLS have already been suggested to be used in bone TE [7,8], cartilage TE [9] and cardiac TE [10].

Prior to device fabrication, suitable SLS process parameters, such as laser power, scan speed, scan spacing, layer thickness, laser beam diameter, and part bed temperature (i.e. temperature in the build chamber) have to be identified [2]. The effects of these parameters on the sintering outcome are interdependent, as well as material dependent, making it challenging to define the ideal sintering conditions for a specific application. Tan and colleagues, for example, investigated the feasibility of sintering for a number of biocompatible polymers, including PCL [11]. In their study, the effects of laser power, scan speed, and part bed temperature variations on melting behaviour were analysed and the authors suggested 2-3 W, 3810 mm/s, and 40°C, respectively, to be the optimal parameters for PCL (Table 1). In further studies, a set of scaffolds produced with the recommended optimal parameters were tested for cytotoxicity and mechanical behaviour [12]. Partee and colleagues studied variations of

laser power, scan speed, scan spacing, part bed temperature and delay in new powder deposition with the aim of obtaining fully dense parts, which were not only dimensionally accurate, but also easily removed from the surrounding unsintered powder [13]. As a result, they proposed two sets of parameters, one for solid parts and one for porous parts (Table 1). Objects produced with the suggested SLS parameters were mechanically characterized in a subsequent study [14]. Lohfeld and colleagues aimed at producing PCL scaffolds with 500 µm strut diameter and tried different scan modalities, as well as different laser power, part bed temperature and number of consecutive scans [15]. The best dimensional accuracy was achieved by having a single scan, with the laser scanning first the outline of the object, then filling the core with a half-strut-thickness offset. Values of the other parameters are listed in Table 1.

Table 1: SLS process parameters for PCL as reported in literature.

LASER POWER (W)	SCAN SPEED (mm/s)	SCAN SPACING (µm)	PART BED TEMPERATURE (°C)	OTHERS	REFERENCE
2-3	3810	N.A.	40	N.A.	[11]
3-4	5080	N.A.	40	N.A.	[16]
4.1	1079.5	152.4	46	Delay in new powder deposition: 0 s (solid parts) 8 s (porous parts)	[13]
4	N.A.	N.A.	38	Number of consecutive scans: 1	[15]

N.A. = Not available

In these studies, however, only dimensional accuracy was considered as the primary factor in defining the most suitable SLS process parameters. The mechanical properties of the sintered objects were measured only after the identification of SLS process parameters. Therefore, these studies do not provide insights into how the SLS process parameters, individually and in combination, influence the mechanical behaviour of sintered objects. However, when employing SLS to produce TE scaffolds, the scaffold mechanical properties are of particular importance. This is the case, for example, for bone TE, where scaffolds should be completely

or at least partially load bearing [17]. Additionally, bone TE scaffolds should have a high and interconnected porosity to allow cell invasion and to promote oxygen and nutrients exchange; however, the fulfilment of the porosity requirement usually results in low mechanical properties [17]. The production of mechanically stable scaffolds with suitable and reproducible porosity is one of the challenges currently faced by bone TE. Mechanically optimized bone TE scaffolds manufactured by AM techniques, such as SLS, have the potential to comply with both mechanical and structural needs.

Here, we aim at developing SLS process parameters to produce PCL scaffolds for bone TE that are not only dimensionally accurate, but also mechanically stable. To the best of our knowledge, such a combined optimization has not been performed on PCL scaffolds before. To achieve our aim, we first compared PCL powders with two different molecular weights and two different particle size distributions concerning their behaviour during SLS and we evaluated the effect of the sterilization method on scaffold mechanical properties. Subsequently, we systematically varied laser power (P_L), laser beam compensation (*BC*) and laser beam diameter (*BD*). The influence of these parameters on mechanical stability and dimensional accuracy of the resulting highly porous scaffolds (>70% porosity, Figure 1A) was investigated by quantifying the compressive elastic modulus (E), the strut diameter (D_S) and the cross-sectional area of the molten core (A_M) inside of the struts. Importantly, the intended use of the here studied scaffold will be in combination with an external fixator, as bone-like stiffness is challenging to achieve with a purely polymeric approach. Finally, the cytocompatibility of PCL scaffolds produced with six different sets of SLS process parameters was studied *in vitro* by eluate tests with primary human mesenchymal stromal cells (hMSCs). The chosen cell phenotype is of relevance for the intended use of the scaffolds in bone TE, as hMSCs are the progenitor cells that differentiate into the cell phenotype involved in new bone formation, i.e. osteocytes [18].

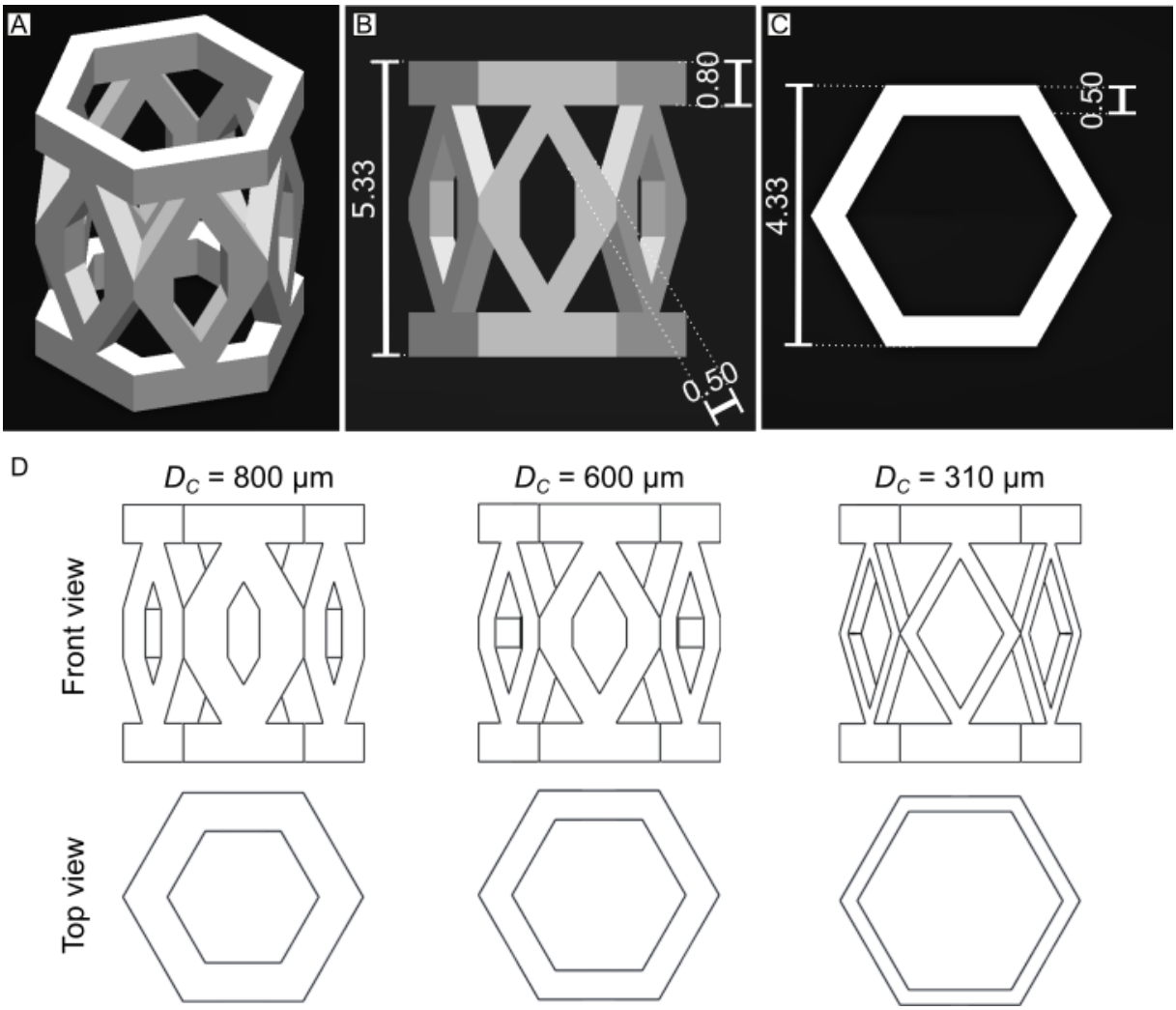

Figure 1: CAD model of scaffold for bone TE. A) Isometric view; B) front view; C) top view; D) Examples of CAD with different strut diameter for in silico analysis. Left, middle and right columns show geometries with strut computational diameter (D_C) of 800, 600 and 310 µm, respectively. All reported values are in mm if not specifically stated otherwise.

2. Materials and Methods

2.1 Scaffold design

A bone TE scaffold with 73.3% porosity and 500 µm strut diameter was designed using SolidWorks (Dassault Systèmes, France) (Figure 1A, B, and C). The design was intended as one structural unit of a larger scaffold, which will be composed of a honeycomb of these individual units. Thus, the scaffold here studied had a hexagonal cross-section.

2.2 PCL powders

PCL powder particles with 60,000 and 100,000 g/mol number average molecular weight ($\overline{M}_n$) and particle size distribution of 25–50 µm were purchased from Aqtis Medical BV

(Netherlands). Additionally, particles with $\bar{M}_n$ of 60,000 g/mol and particle size distribution of 50–80 µm were acquired from the same supplier. For each particle type, at least N = 3 scaffolds were produced by SLS with P_L = 0.4 W, *BC* = 200 µm and BD = 390 µm and mechanically characterized as described below.

2.3 SLS process

The bone TE scaffold was produced by SLS using a laboratory SLS machine equipped with an ionizer to prevent powder agglomeration. P_L, *BC* and *BD* were varied as listed in Table 2. P_L is the power that the laser applies to the material. *BC* is a geometric parameter: the laser starts scanning the material with an offset *BC* from the border of the designed object to compensate for the width of the melting track. *BD* is the size of the laser beam that scans the material. The other sintering parameters were kept constant at the following values: 50 mm/s scan speed, 67° scan pattern rotation between layers, unidirectional scans, 20 µm hatch distance, 50 µm layer thickness. For each set of SLS parameters, at least N = 3 scaffolds were produced from PCL particles with $\bar{M}_n$ of 60,000 g/mol and 50–80 µm particles size distribution and mechanically characterized as described below. After the SLS process, the scaffolds were treated with compressed air (2 bar for 10 s) to remove loosely attached particles.

*Table 2: Investigated SLS process parameters: laser power (**P_L**), laser beam compensation (BC) and laser beam diameter (BD).*

***P_L* (W)**	***BC* (µm)**	***BD* (µm)**
0.30	150	260
0.35	200	390
0.40	205	
0.45	210	
0.50	225	
0.60	230	
0.70		

2.4 Scaffold sterilization

N = 9 scaffolds were produced with P_L = 0.40 W, *BC* = 200 µm, and *BD* = 260 µm. From these, N = 3 scaffolds were randomly chosen to be sterilized by ethylene oxide (EtOx), N = 3 by gamma (γ) irradiation, and N = 3 were kept unsterile as reference. Sterilization was performed by HA2 Medizintechnik GmbH (Germany). Sterilized and reference scaffolds were mechanically characterized as described below.

2.5 Morphological characterization

Morphological characterization was performed by measuring height and width of the produced scaffolds with a digital calliper (DigitCal, Tesa, Switzerland). The strut diameter (D_S) was measured from light microscope images (SMZ1270, Nikon, Japan) using the software NIS-Elements D 4.30.02. The measurement of D_S was performed on the four struts of each one of the six faces of the scaffolds, as exemplarily shown in Figure 4B.

To evaluate the morphology of the strut cross-section, scanning electron microscopy (SEM) was performed using a JCM-6000 machine (Jeol, Japan). For SEM, N = 1 scaffolds per type were prepared by embedding in TissueTek® (Sakura Finetek Europe B.V.) and cryocut to ¾ of their height at -20°C with a Leica CM3050 S cryomicrotome (Leica, Germany) using a slice thickness of 20 µm. TissueTek® was removed by repeated washings in deionized water. Scaffolds were dried at room temperature for one day, then gold sputtered for 30 s at 8 Pa pressure and 40 mA electrical current prior to SEM imaging. The molten cross-sectional area (A_M), defined as the region in which particles were completely molten during the SLS process and re-solidified in a compact area, was measured from SEM pictures of individual struts using Fiji (ImageJ, NIH) (**Errore. L'origine riferimento non è stata trovata.**H). For each sample, N = 12 strut cross-sections were measured. The molten cross-sectional diameter (D_M) corresponding to A_M was calculated as the diameter of a circular cross-section using equation (1):

$$D_M = 2\sqrt{\frac{A_M}{\pi}} \quad (1)$$

Results are reported as average ± standard deviation.

2.6 Mechanical characterization

Scaffolds were mechanically tested in monoaxial compression using a BOSE Test Bench (LM1 TestBench, TA Instrument ElectroForce System Group, USA) equipped with a 222.5 N load cell. During the test, applied displacement and measured reaction force were recorded and subsequently used to calculate the stress-strain curves. The compressive elastic modulus (E) was obtained by a linear fit of the elastic region of the stress-strain curves. At least N = 3 scaffolds per type were tested.

Results are reported as average ± standard deviation.

2.7 Molecular weight characterization

The molecular weight distribution of raw powders and of sterilized and reference scaffolds was measured by a size exclusion chromatography instrument (Agilent Technologies 1200 Series,

USA) equipped with a refractive index detector, according to Boffito et al. [19]. Briefly, materials were dissolved at 2 mg/ml concentration in a solution of N,N-dimethylformamide (Chromasolv HPCL grade, CarloErba Reagents, Italy) added with lithium bromide (Sigma Aldrich, Italy) at 0.1% w/v and filtered using a 0.45 µm poly(tetrafluoroethylene) syringe filter (Lab Logistic Group GmbH, USA). Then, the analysis was performed at 55°C with a flow rate of 0.5 ml/min through two Waters Styragel columns (HR1 and HR4). Finally, number average molecular weight ($\bar{M}_n$), weight average molecular weight ($\bar{M}_w$) and dispersity index ($DI = \bar{M}_w/\bar{M}_n$) were estimated using the Agilent ChemStation Software and a calibration curve based on poly(methyl methacrylate) (PMMA) standards ($\bar{M}_n$ ranging from 4,000 to 200,000 g/mol).

2.8 In silico analysis of scaffold elastic modulus as function of strut diameter

The theoretical relationship between elastic modulus and strut diameter was assessed by computational analysis. A variation of scaffold strut diameter in dependency of SLS process parameters was experimentally observed. To reproduce these experimentally measured strut size variations, six additional CADs were prepared in SolidWorks (Dassault Systèmes, France). The CADs had the same architecture as the produced scaffold, but their strut diameter was 310, 400, 500, 600, 700 and 800 µm (Figure 1D). The CADs had square cross-sections to be consistent with the original CAD design, but, as they were used to give a computational representation of the experimental irregular cross-section of the struts, the cross-sectional thickness of the CADs will be named computational diameter (D_C). The six scaffold geometries with varying strut diameter were not fabricated by SLS, but they were evaluated in compression by finite element (FE) analysis using Abaqus (Dassault Systèmes, France). Scaffold geometries were meshed with a tetrahedral mesh with seed size of 0.15 mm and assigned elastic material properties of the bulk material with compressive modulus of 70 MPa and Poisson's ratio of 0.3. The *in silico* scaffold material properties were derived by running FE analyses with different material values and selecting the set of values that best matched the experimental data. An encastre boundary condition was imposed to the bottom face of the geometry and an axial 3% compressive displacement was applied to the top face, simulating the compressive test experimentally performed. This range of compressive displacement was expected to be within the region of elastic behaviour of the scaffolds. The reaction force (*RF*) of each CAD was calculated and used to evaluate the computational elastic modulus (E_C) with equation (2):

$$E_C = \frac{\sigma}{\varepsilon} = \frac{RF}{A_C} \cdot \frac{L_C}{\Delta L_C}\,, \qquad (2)$$

where σ is the stress, ε is the strain, A_C is the CAD hexagonal cross-section, L_C is the CAD height and ΔL_C is the applied displacement.

2.9 Cytocompatibility test

Six scaffold prototypes ("A" to "F", Table 4) were tested for cytocompatibility of the eluate with primary human mesenchymal stromal cells (hMSCs).

Cells were obtained by density gradient separation from the bone marrow of patients undergoing total hip replacements. The use of primary human bone marrow mesenchymal stromal cells was approved by the ethics committee of the Charité–Universitätsmedizin Berlin, and donors' written informed consent was given. Cell culture was performed in expansion medium composed of Dulbecco's modified Eagle's medium (DMEM, Sigma, 1000 mg/l glucose), 10% foetal bovine serum (FBS, Biochrom AG), 1% penicillin/streptomycin (P/S, Biochrom AG), 1% L-glutamine (glutaMAX, Invitrogen). Cells were trypsinized (PAA Laboratories GmbH) at approximately 80% confluency and experiments were carried out with cells in passages 3 or 4.

Batches of conditioned medium were prepared by placement of the prototypes in 3 ml of expansion medium and by incubation at 37°C and 5% CO_2 for at least 24 hours before exposure to cells. Specifically, cells of the day 3 and 6 time points were exposed to medium conditioned for 24 hours and 3 days, respectively. At each experimental time point, a maximum of 1200 µl (specifically, 200 µl/well) of conditioned medium was taken from each batch to be used in cell culture. The same volume that was removed was subsequently refilled with fresh expansion medium.

Cells were seeded in 48-well plates with a confluency of 30%. At day 0, i.e. 24 hours after seeding, and 3, hMSCs were exposed to 200 µl of conditioned medium. Cells cultured in 200 µl of expansion medium were used as controls. Medium evaporation was reduced by surrounding the cell-seeded area with wells filled with 600 µl of phosphate buffered saline (PBS, Gibco, Life Technologies Limited), which were refilled at day 3. At day 0, 3 and 6, AlamarBlue (#DAL 1100, Invitrogen) and Cyquant (#C7026, Thermo Fisher Scientific) assays were performed to assess cellular metabolic activity and number, respectively. For each tested condition, 3 wells/time point were seeded, with the exception of the day 0 time point, which consisted of 6 control wells. Four independent repetitions of the experiment were performed. To reduce the risk of introducing systematic errors by pipetting order or by sample position in the well plate (e.g. edge effects due to non-uniform environmental conditions at the border of the cell-seeded area), the position of the wells conditioned with the six media and of the control wells was randomly varied at each repetition. Results of the AlamarBlue and Cyquant assays were evaluated with an Infinite M200 Pro plate reader (Tecan).

During the result analysis of each experimental repetition, outliers in the raw data were identified within the 3 wells of each condition. The average of the two wells having the highest fluorescence intensity values was taken as reference and the intensity of the third well was

calculated as percentage of the reference. If the resulting percentage was lower than 50%, the third well was considered an outlier and removed from the data set. Similarly, outlier values between the experimental repetitions were identified by calculating the percentage of the repetition with the lowest average value in respect to the average of the other three repetitions. Also in this case, a percentage lower than 50% was considered an outlier.

Statistical significance was tested between the control and each investigated condition by means of a two-sided Mann-Withney-U test performed in Origin 2019b (OriginLab Corporation). Values of $p < 0.05$ were considered as statistically significant, while values of $p > 0.05$ were considered as non-significant.

Values were normalized to day 0 and are given as average ± standard deviation of fold change.

3. Results and Discussion

3.1 Influence of PCL powders on scaffold mechanical properties

Size exclusion chromatography (SEC) was performed on PCL powders to study their molecular characteristics and to serve as a reference for the subsequent evaluation of how the SLS process would influence the properties of PCL. The number average molecular weight and dispersity index resulting from the SEC analysis are shown in Table 3.

Table 3: Number average molecular weight and dispersity index of the different raw materials and powder-based scaffolds investigated in this study. All scaffolds were produced from the PCL powder with nominal molecular weight of 60,000 g/mol and particle size distribution of 50–80 µm.

SAMPLE TYPE	PARTICLES SIZE DISTRIBUTION (µm)	NUMBER AVERAGE MOLECULAR WEIGHT (g/mol)	DISPERSITY INDEX
Powder – low molecular weight	25–50	59,800	1.85
Powder – high molecular weight	25–50	95,500	1.84
Powder – low molecular weight and larger particle diameter	50–80	57,600	1.81
Scaffold - Unsterile	50–80	55,000	1.80
Scaffold - EtOx	50–80	57,700	1.80
Scaffold - Gamma	50–80	37,700	2.20

Mechanical testing showed that higher molecular weight PCL particles yielded scaffolds with lower *E*. In fact, SLS of lower (60,000 g/mol) and higher (100,000 g/mol) molecular weight particles, but equal particles size of 25–50 µm, resulted in scaffolds with $E_{S,60}$= 11.3 ± 0.5 MPa and $E_{S,100}$= 5.6 ± 1.2 MPa, respectively. The elastic moduli values were normalized to the elastic modulus of the scaffold produced from particles having molecular weight of 60,000 g/mol and size of 25–50 µm to better highlight the differences between groups (Figure 2A). In general, semi-crystalline polymers, such as PCL, tend to be more ductile and stronger at high molecular weights, as the polymeric chains with low molecular weight tend to collect in between crystalline regions, thereby lowering the number of "tie molecules" [20]. Thus, semi-crystalline polymers with low molecular weight tend to be brittle and have low strength, while those with high molecular weight tend to have a higher toughness [20]. Therefore, it could be expected to obtain higher *E* scaffolds using a higher molecular weight polymer, as it was shown for PCL scaffolds produced by 3D-printing and tested in compression [21]. However, the higher the molecular weight of PCL is, the higher is the viscosity of the molten polymer [22]. Consequently, the lower *E* measured for the higher molecular weight scaffolds might be explained by a lower sintering rate resulting from the higher melt viscosity [23,24]. Moreover, the crystallinity of PCL was shown to decrease with increasing molecular weight, contributing

to the production of specimens with lower *E* [25]. In the scaffolds produced from the PCL powder with the higher molecular weight (Figure 2F), more loosely attached powder particles were observed compared to the scaffolds produced from the powder with lower molecular weight (Figure 2E and G). This might be ascribed to the lower crystallinity of the high molecular weight PCL, which could lead to more necking next to the scanning path of the laser.

The deposition of an evenly distributed layer of powder platform is an important premise for a robust and reproducible SLS process. In this context, powder behaviour during deposition is described by its flowability, defined as the powder ability of flowing in a desired manner in a specific piece of equipment [26]. Powder flow during the SLS process was remarkably different for the two powders with the same molecular weight of 60,000 g/mol but different particle size. Bigger particles of 50—80 µm were homogeneously spread by the roller, which was additionally equipped with an ionizer to avoid particle aggregation (Figure 2B), while smaller particles of 25—50 µm formed aggregates despite the presence of the ionizer (Figure 2D). During the movement of the roller from the powder reservoir to the building platform and back, such aggregates dropped randomly onto the deposited powder layer, thereby impairing a uniform powder distribution. If a powder aggregate would be on the laser path during the sintering process, the locally increased layer thickness would cause this specific object area to have different properties from the neighbouring ones. Thus, the reproducibility of the technique would be impaired. These observations are consistent with literature, where it was reported that powders consisting of particles with diameter smaller than 45 µm have unfavourable flow properties due to high electrostatic forces [2]. Nevertheless, scaffolds were produced successfully with the two particle sizes and their mechanical characterization revealed a comparable elastic modulus of E= 11 MPa (Figure 2A). Because of the identical mechanical stiffness of the resulting scaffolds and the favourable flowability, the PCL powder with 60,000 g/mol molecular weight and 50–80 µm particles size was selected to produce the scaffolds for all subsequent experiments.

3.2 Influence of sterilization on mechanical properties

Sterilization is particularly relevant when planning the production of TE devices [17]. Importantly, the chosen sterilization method should not significantly alter the properties that were engineered for the specific device. For this reason, we tested two different sterilization methods, namely ethylene oxide (EtOx) and gamma (γ) irradiation, and we evaluated their influence on scaffold elastic modulus and PCL molecular weight. By performing these sterilization tests at the first stages of scaffold development, we ensured that the subsequent

fine-tuning of scaffold properties could be maintained throughout the device processing until its actual application.

Mechanical properties of unsterile, EtOx- and γ-sterilized scaffolds were found to be similar, with values of E_S= 20.9 ± 1.9, $E_{S,EtOx}$ = 18.1 ± 1.2, and $E_{S,\gamma}$ = 18.6 ± 3.0 MPa, respectively. Elastic moduli values were normalized to the elastic modulus of the unsterile scaffold to better highlight differences between groups (Figure 2C). However, SEC analysis revealed a large 35% decrease in molecular weight for γ-sterilized scaffolds (Table 3), with a reduction in number average molecular weight from $\bar{M}_{n_{pow}}$= 57,600 g/mol (raw powder) to $\bar{M}_{n_{S,\gamma}}$= 37,700 g/mol (γ-sterilized scaffold). The observed variation in molecular weight was significant, as the usual error of SEC analysis is approximately 10% [27]. At the same time, the dispersity index increased from 1.80 to 2.20 (Table 3). On the contrary, the number average molecular weight of EtOx sterilized scaffolds was $\bar{M}_{n_{S,EtOx}}$= 57,700 g/mol, similar to both the raw powder ($\bar{M}_{n_{pow}}$= 57,600 g/mol) and the scaffold before sterilization ($\bar{M}_{n_S}$= 55,000 g/mol) (Table 3). Raw powder, unsterile and EtOx sterilized scaffolds had also equal dispersity index of 1.80 (Table 3).

Various effects of γ irradiation on PCL have been reported in literature. For example, a reduction in molecular weight and in tensile stiffness and strength was observed in PCL electrospun membranes [28]. In another study, γ irradiation of PCL films resulted in larger tensile yield points and lower number average but higher weight average molecular weight, indicating both crosslinking and chain scissions [29]. Furthermore, no remarkable differences in tensile mechanical behaviour was measured in γ-sterilized PCL electrospun membranes, but at the same time there were indications of chain scission [30]. Taken together, these studies suggest a controversial relationship between γ-irradiation and PCL mechanical properties. However, a clear impact on the polymer molecular weight can be concluded, in agreement with our findings. Although there was no obvious immediate effect on the compressive elastic modulus, the reduction in molecular weight caused by γ-sterilization might have an impact on PCL degradation speed, and thereby on long-term scaffold stability. For example, PCL films were produced with different ratios of high and low molecular weight polymer and the films having a higher amount of low molecular weight chains were shown to have a greater *in vitro* weight loss after 21 weeks [31]. Furthermore, PCL undergoes a two-stage degradation *in vivo*, in which each phase is determined by the molecular weight [32]. First, long polymeric chains are cleaved by hydrolysis [6]. Second, PCL fragments smaller than 3,000 g/mol undergo intracellular uptake [33] and are eventually excreted through faeces and urine [32]. The *in vitro* degradation behaviour of the PCL scaffolds was not investigated in this work. Previous studies showed that specimens with an even lower molecular weight showed no significant degradation over a timeframe of up to three months. Specifically, electrospun

PCL membranes with number average molecular weight of 15,000 g/mol showed no changes in molar mass after 100 days of immersion in phosphate buffered saline (PBS) [34]. In another case, PCL films with an initial number average molecular weight of 17,000 g/mol were degraded in PBS and simulated body fluid (SBF) for 90 days, resulting in a maximum mass loss of 3% and a reduction in molecular weight of 13% in PBS [35]. The *in vivo* degradation of the scaffolds is expected to be in the range of 2 to 4 years depending on the initial molecular weight [6]. For a translational approach, the material degradation should be evaluated at the specific site of scaffold implantation to gain insights into PCL degradation in the according environment.

Considering the performed observations, EtOx was selected here as the preferred sterilization method, since it altered neither the molecular weight of the polymer nor the mechanical properties of the scaffold.

3.3 Influence of SLS parameters on scaffold properties

After identifying which PCL powder was most suitable for the SLS process and evaluating the least material-altering sterilization method, a systematic SLS parameter variation was performed to investigate effects on the mechanical and morphological properties of the produced scaffolds. An identical scaffold design (Figure 1A) was produced with different SLS parameters (Table 2). The elastic modulus (E) and strut diameter (D_S) in dependency of laser power (P_L), beam compensation (BC) and beam diameter (BD) variations are shown in Figure 3.

Depending on the parameter set, the stiffness of PCL scaffolds varied by a factor of 18.9 from values as low as E = 1.76 ± 0.05 MPa to as high as E = 33.33 ± 2.27 MPa. Moreover, the resulting strut diameter D_S ranged from approximately 400 to 800 µm, whereas the designed strut diameter was 500 µm in all cases (Figure 1A, B, and C).

As discussed above, SEC analysis of sintered material showed no PCL degradation due to the SLS process (Table 3), as opposed to the circa 20% reduction in post-sintering molecular weight reported in literature [14]. This different material behaviour might be ascribed to gentler temperature-time cycles employed in the present study, as a low scan speed (50 mm/s) and no preheating were used here (c.f. Table 1).

Part bed preheating has been suggested in literature to minimise not only powder thermal expansion due to the laser, but also shrinkage of semi-crystalline polymers, such as PCL, during recrystallization in the cooling phase, thereby avoiding the sintered piece to curl and be deformed during production [2]. Even though the part bed was at room temperature, all scaffolds in the present study were successfully produced without deformation. However, it was necessary to use a substrate material as base plate, as it is known from laser powder bed fusion of metals. Moreover, the absence of part bed heating might have contributed to the

here-observed absence of polymer degradation through a shorter exposure of the material to high temperatures. However, the transferability of the findings to larger scaffolds might be difficult as curling effects are a matter of part size.

Systematic parameter variations showed that the same mechanical properties of the sintered scaffolds could be achieved with multiple sets of SLS parameters (Figure 3). Even though a certain scattering of the data was observed, there was a dominating dependency between the scaffold elastic modulus E and the strut diameter D_S. In fact, different parameter sets resulted in scaffolds with comparable E only if D_S was similar. Therefore, we concluded that the SLS parameters influenced the mechanical properties of scaffolds mostly to the extent to which they influenced the strut diameter D_S.

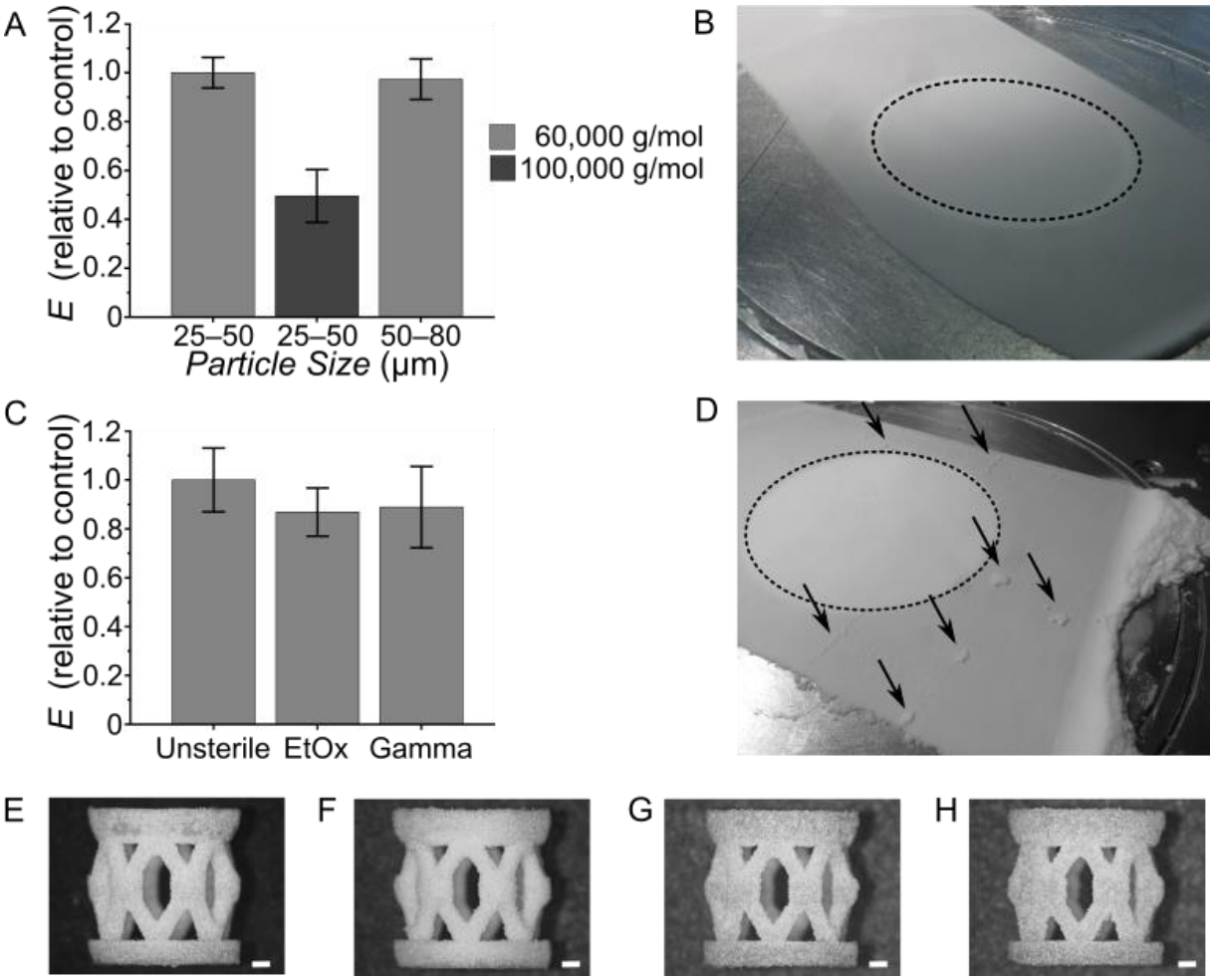

Figure 2: Influence of PCL powder and sterilization method on scaffold elastic modulus and SLS process. A) Elastic modulus ratio of scaffolds produced with 60,000 and 100,000 g/mol molecular weight particles and with particle size of 25–50 and 50–80 µm. Values were normalized to the elastic modulus of the control, which were the scaffolds produced from PCL particles with molecular weight of 60,000 g/mol and size of 25–50 µm; B) deposition of powder with particle size of 50–80 µm and 60,000 g/mol molecular weight. The black dashed circle marks the building platform (diameter 70 mm); C) elastic modulus ratio of unsterile, EtOx- and γ-sterilized scaffolds. Values were normalized to the elastic modulus of the control, which were the unsterile scaffolds; D) deposition of powder with particles size of 25–50 µm and 60,000 g/mol molecular weight. The black dashed circle marks the building platform (diameter 70 mm). Arrows indicate powder aggregates; E), F) and G) representative pictures of scaffolds produced with "25–50 µm and 60,000 g/mol", "25–50 µm and 100,000 g/mol" and "50–80 µm and 60,000 g/mol" particles, respectively; H) representative picture of unsterile scaffold from the batch that underwent sterilization. Scale bars are 620 µm.

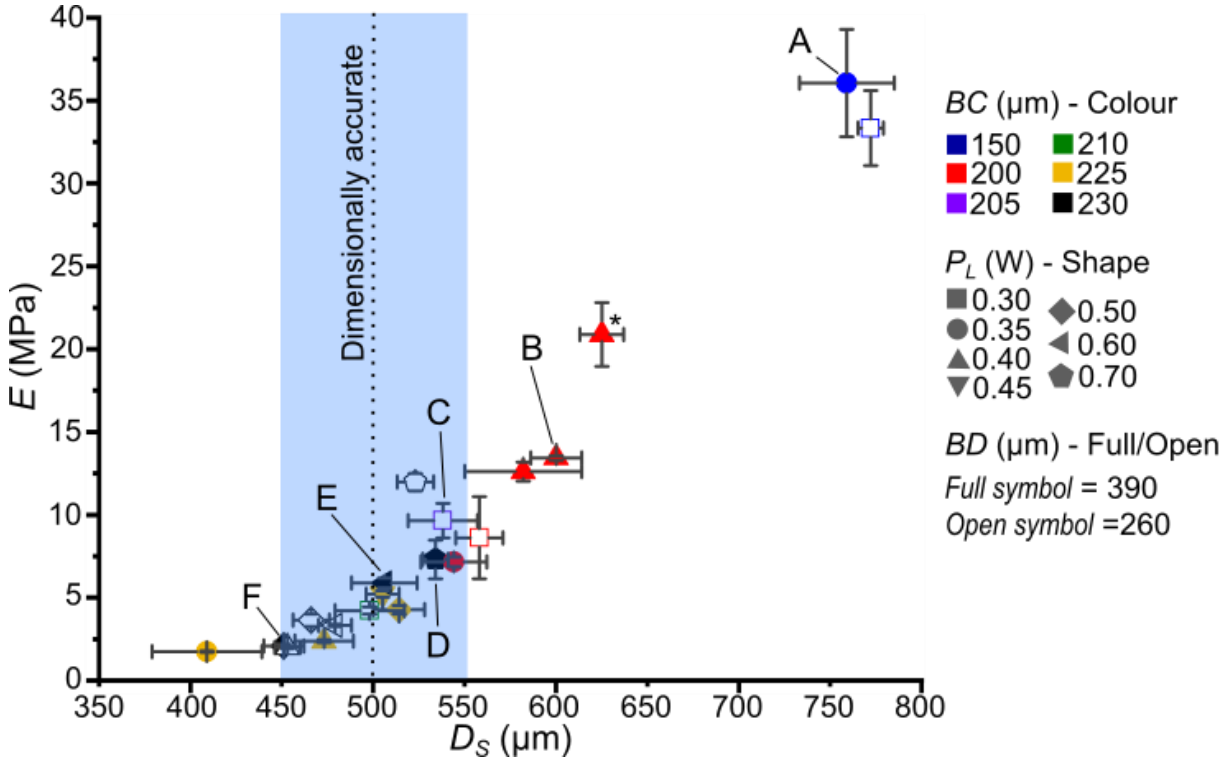

Figure 3: Influence of laser power (P_L), beam compensation (BC) and beam diameter (BD) variations on scaffold elastic modulus (E) and strut diameter (D_S). Colours, shapes and full/empty contours indicate different BC, P_L and BD, respectively. The dotted line shows the CAD strut diameter of 500 µm. The blue shaded area is the diameter range that was considered as sufficiently accurate. Prototypes "A" to "F" are marked in the plot and were further investigated. The asterisk marks the scaffold that was used as unsterile control in the sterilization test.

3.4 Influence of SLS parameters on scaffold morphology

To better understand the relationship between strut diameter and mechanical properties, six prototypes ("A" to "F", see Table 4) were selected from the many parameter combinations shown in Figure 3Figure 2 for a more detailed analysis. Selection criteria were based on

- high elastic modulus despite low dimensional accuracy (prototypes "A" and "B", Figure 4A and B, respectively);
- high dimensional accuracy despite low elastic modulus (prototypes "D", "E", and "F", Figure 4D, E, and F, respectively);
- good compromise between dimensional accuracy and elastic modulus (prototype "C", Figure 4C).

Table 4: SLS parameters and resulting properties of prototypes that were selected for morphological analysis.

Type	Parameter	Prototype A	Prototype B	Prototype C	Prototype D	Prototype E	Prototype F
Laser sintering parameters	P_L (W)	0.35	0.40	0.30	0.70	0.60	0.40
	BC (µm)	150	200	205	230	230	230
	BD (µm)	390	260	390	390	390	260
Scaffold properties	D_S (µm)	759	600	538	534	506	453
	E (MPa)	36	13	10	7	6	2

The selected scaffolds were representative prototypes of different SLS parameter sets as shown in Table 4. Moreover, the selected prototypes covered well the observed broad range of strut diameter and mechanical stiffness. The strut molten cross-sectional area A_M, defined as the region in which the material was fully molten during the SLS process and individual particles were not distinguishable anymore, was evaluated from the SEM images of individual struts (Figure 4H). To do so, the selected prototypes were cryocut to ¾ of their height, as schematically shown in Figure 4G, and imaged by SEM. The quantification of A_M (Figure 4I) revealed that the molten cross-sectional area greatly varied depending on the SLS parameters, ranging from A_M = 0.01 ± 0.01 to 0.32 ± 0.03 mm^2 (Figure 4J to O), although all scaffolds were produced from the same CAD with designed cross-sectional area A_M of 0.29 mm^2 (Figure 4G). Interestingly, for dimensionally accurate scaffolds, i.e. scaffolds whose D_S was close to the design value of 500 µm, a fully molten cross-section was not necessarily found within every strut. This effect was particularly clear in scaffolds with small D_S, such as prototype "F" (Figure 4O) and pointed to a certain degree of variability within the same printing process (intra-process variability). Variability was also observed between different printing processes (inter-process variability), where scaffolds produced with the same SLS parameters, but at different times, showed slightly different properties (see upright red triangles with full shape in Figure 3). The maximum recorded inter-process variations of *E* and D_S were 40% and 7%, respectively. Such inter- and intra-process variability has been discussed in literature as a characteristic feature of laser sintering and melting production techniques and it has been described for their application to different materials, such as semi-crystalline polymers [36] and metals [37]. The origins of the variability are numerous, but they can be ascribed both to material-dependent [36] and to process-dependent [36,37] aspects. A detailed discussion on SLS variability sources, however, is beyond the scope of this work. Despite the SLS intrinsic variability, relevant observations could be performed on the analysed scaffolds. In fact, quantification of the molten cross-sectional area showed that scaffolds whose D_S was close to 500 µm generally had A_M ranging from 0.01 ± 0.01 to 0.13 ± 0.01 mm^2, i.e. 97% to 55% lower than the design value of 0.29 mm^2, respectively (Figure 4I).

The strut molten cross-sectional diameter D_M was calculated from A_M using equation (1). Even though the original CAD design had a square cross-section (Figure 1), the calculation of D_M as the diameter of a circular cross-section was more appropriate for the observed shape of the molten cross-sectional area (Figure 4J to O). Evaluating the strut diameter from light microscope images is common practice in literature [13,15] but it clearly over-estimates the dimension of the fully molten cross-section represented here by D_M.

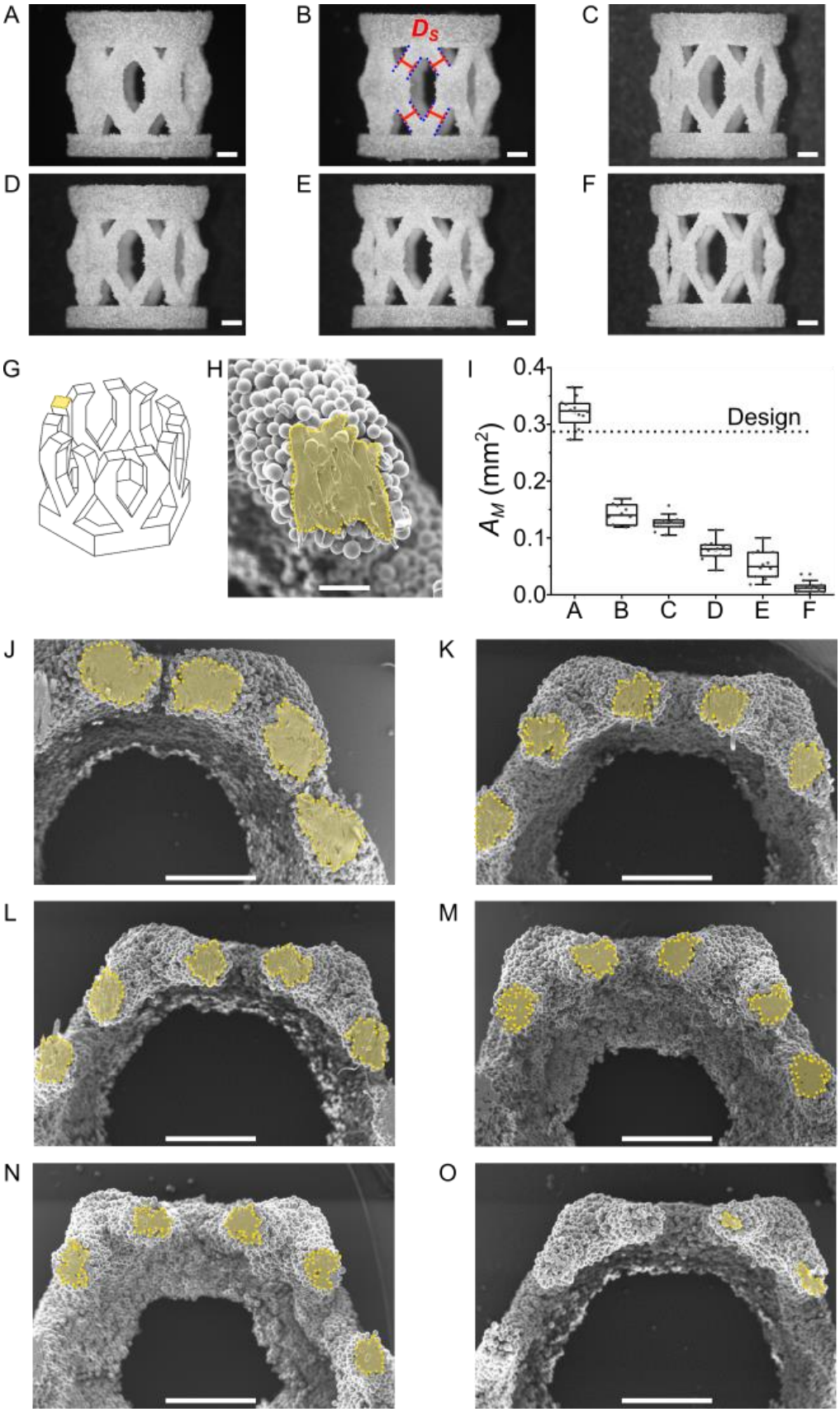

Figure 4: Results of morphological evaluation. A) to F) light microscope pictures. Image labels correspond to prototype names. Scale bars are 800 µm. An example of strut diameter (D_S) measurement is shown in B); G) CAD representation of the cut scaffold. The design reference

A_M is highlighted; H) representative SEM image used for A_M quantification. The dotted line marks the A_M of the strut. The scale bar is 200 µm; I) quantification of A_M of analysed prototypes. The dotted line indicates the reference A_M of the design with value of 0.29 mm^2; J) to O) overview SEM images of prototypes "A" to "F", respectively. The dotted lines mark the A_M of individual struts. Scale bars are 1 mm.

As the scaffold architecture with inclined and crossing struts leads to a complex deformation behaviour under compression, a straightforward prediction of how the scaffold stiffness would depend on strut diameter was not possible. Thus, the principle relationship between elastic modulus and strut diameter was derived using an *in silico* approach (i.e. via computational analysis) for a later comparison with the experimental results. It is worth mentioning that the *in silico* method provided insights into how the scaffold would behave mechanically if all powder was molten into a compact material, representing the ideal situation where D_M equals D_S. The experimentally observed variation of strut diameter resulting from the different SLS parameter sets was represented by six CADs having the same principle geometry as the produced scaffold, but different strut diameters ranging from 310 to 800 µm (exemplarily shown in Figure 1D), as motivated by the experimentally observed strut diameters (400–800 µm). These geometries were used to study the theoretical dependency between elastic modulus and strut diameter by finite element (FE) analysis. Each CAD underwent a FE evaluation in compression, from which the computed elastic modulus (E_C) was calculated using equation (2). The relationship between elastic modulus E_C and strut computational diameter D_C was found to follow a quadratic polynomial expressed by equation (3) (Figure 5A).

$$E_C = 7.2 \cdot 10^{-5} D_C^2 \qquad (3)$$

Where the factor $7.2 \cdot 10^{-5}$ had units of MPa/µm^2. Equation (3) was subsequently used as fit-function for the experimentally derived data. To do so, a pre-factor K was introduced to correct for the unknown elastic modulus of the sintered PCL material, which was an ad-hoc assumption in the *in silico* approach.

The *in silico*-derived fit function with a pre-factor K = 1.05, as stated in equation (4), matched well the experimental data points when expressing scaffold elastic modulus as function of the molten cross-sectional diameter $E(D_M)$ with $R^2 = 0.9997$ (Figure 5B).

$$E = K \cdot 7.2 \cdot 10^{-5} \cdot D_M^2 \quad \text{with } K = 1.05 \qquad (4)$$

On the contrary, there was a strong disagreement between the *in silico*-predicted dependency and the analysed dependency between scaffold elastic modulus and the outer strut diameter $E(D_S)$ indicated by a low value $R^2 = 0.32$. The data could be fitted through the polynomic function shown in equation (5), but it was not in agreement with the theoretical requirement that an elastic modulus $E = 0$ would be reached at zero strut diameter. In contrast, $E = 0$ was already reached at $D_S \approx 400$ µm (precisely at $D_S = 428$ µm) according to equation (5) (see also Figure 5B). This roughly corresponds to the resolution limit of the SLS process, which depends on laser beam diameter and heat conduction.

$$E = -2.6 - 4.1 \cdot 10^{-2} \cdot D_S + 1.1 \cdot 10^{-4} \cdot D_S^2 \quad (5)$$

D_M was consistently smaller than D_S (Figure 5C) and none of the analysed prototypes fulfilled the ideal sintering case, where D_M would be equal to D_S. However, prototypes showed an asymptotic trend to a line that represented a situation where D_S was larger than D_M by a constant value of 100 µm (grey dotted line in Figure 5C), as described by equation (6):

$$D_S = e^{6.1+3.9\cdot10^{-4}\cdot D_M+7.8\cdot10^{-7}\cdot D_M^2} \quad (6)$$

For strut diameter >> 550 µm, this might be a constant factor representing a layer of partially sintered particles with a thickness of 50 µm (≈ 1 particle diameter) surrounding the molten cross-section. However, this layer was found to be over-proportionally thick for strut diameters < 550 µm, as the curve deviated strongly towards larger values of D_S for decreasing D_M, approaching $D_S = 428$ µm for $D_M = 0$ (black fit curve in Figure 5C).

To better illustrate how the layer thickness of partially sintered particles increases with decreasing diameter of the molten cross-section, the ratio D_M/D_S was calculated and plotted as function of D_M (Figure 5D). In this case, six additional data points were extrapolated by assuming an offset of 100 µm (i.e. two times the thickness of the layer of partially sintered particles) between D_S and D_M for diameters >> 550 µm, as derived from the observations reported for Figure 5C. Data point extrapolation was performed to better represent the shape of the curve D_M/D_S for large values of D_M. Data points were fitted well by the function expressed in equation (7), which assumed that the curve would asymptotically approach the value of 1 for D_M approaching an infinite value. Moreover, equation (7) considered that $D_M/D_S \approx 0$ if $D_M = 0$ µm.

$$\frac{D_M}{D_S} = \frac{D_M}{D_M+100} - \frac{0.165}{1+9.7\cdot10^{-9}\cdot D_M^3} \quad (7)$$

584 Generally, the measure of the molten cross-sectional diameter D_M of the sintered scaffolds
585 better explained the observed differences in mechanical stiffness amongst scaffolds with
586 similar strut diameter D_S (see prototypes “C”, “D”, and “E” in Figure 5B). Moreover, D_M better
587 reflected the theoretical relationship between the scaffold mechanical properties and
588 dimensions compared to D_S. A similar observation was reported for the production of lattice
589 structures by selective laser melting from an aluminium alloy, where computational and
590 experimental results matched only if the computational model reproduced the elliptic strut
591 cross-section resulting from the production process, as opposed to the circular cross-section
592 of the CAD [38].
593 Additionally, we observed that the difference between D_M and D_S increased for small strut
594 diameters, while it tended towards a constant value for large strut diameters (Figure 5C). The
595 effect could be clearly visualized by observing the asymptotic behaviour of the data in Figure
596 5C and by expressing the ratio D_M/D_S in function of D_M in Figure 5D. The value $D_M/D_S = 0.8$
597 (molten cross-sectional diameter = 80% of strut diameter) corresponding to D_M = 590 µm was
598 defined to mark the transition between the steep decline of D_M/D_S for $D_M <$ 550 µm and the
599 approximation towards $D_M/D_S = 1$ for values $D_M >$ 550µm. A low value of D_M/D_S indicates that
600 an over proportional amount of powder is only partially sintered and does not contribute in an
601 optimal way to the load-bearing function of the scaffold. This might be a consequence of a
602 reduced heat conduction into the depth of the underlying sintered material, as there is only
603 very little fully fused and compact material beneath the top layer. This compact material,
604 however, can be expected to have a higher heat conductivity than the powder or partially
605 sintered particles and thus would dissipate the heat more effectively. If little compact material
606 is available, more heat might be conducted laterally into the powder bed to partially sinter
607 particles without full melting. This would lead to the comparably large D_S for small D_M observed
608 here.

Our observations indicated that the presence of a molten core with sufficiently large cross-section was the key factor in the production of mechanically stable scaffolds by SLS. Therefore, we suggest optimizing SLS parameters to produce mechanically stable scaffolds by evaluating the strut molten cross-sectional diameter, rather than the strut diameter. We observe that the partially sintered particles attached to the molten cross-section have a low contribution to the mechanical competence of the sintered structure as E(D_M) but not E(D_S) is in agreement with the principle dependency E(D_C) predicted by computational analysis. When evaluating the strut diameter D_S only, one might in fact produce scaffolds that have the exact dimensions of the input CAD file, but fail under even moderate mechanical loading as they might be composed of partially sintered particles only. This finding is particularly relevant when producing scaffolds with small strut diameter, high porosity and high mechanical requirements, as it is generally the case in bone TE. For such applications the ratio between the diameter of the molten cross-section and the diameter of the strut should not deviate strongly from the ideal value of $D_M/D_S = 1$. We here recommend $0.8 < D_M/D_S \leq 1$ for the material type (PCL) and particle size (50–80 µm) used in this study.

The ratio $D_M/D_S = 0.8$ was found to be reached at a molten cross-sectional diameter of $D_M = 590$ µm and a strut diameter of $D_S = 740$ µm, corresponding to 9.1 and 11.4-times the mean powder particle diameter of 65 µm, respectively (powder particle size distribution: 50–80 µm). The production of struts with a diameter above this value is predicted to be a reliable way to obtain scaffolds with high mechanical stiffness, as it can be deduced by equation (4) and Figure 5B. If the appropriate sterilization method is applied (ethylene oxide), mechanically competent and sterile scaffolds can be produced, for which the dispersity index predicts no significant alterations of the polymer during the process (see Table 3).

It has to be mentioned that the threshold diameter of $D_S = 740$ µm defined in this study cannot be generalized to all SLS applications, as the outcome of the sintering process depends on material type, particle size distribution and shape, sintered object geometry, and SLS parameters [36]. While the principle presented here is expected to be generally valid, the minimum feature size needs to be determined experimentally for each specific application. Altogether, the understanding acquired here will help to improve the production of scaffolds for bone TE by SLS, especially when high porosity, small feature size and optimized mechanical properties are targeted.

As an optimal SLS process is strongly material- and design-dependent, we do not intend to offer a final set of optimal parameters for PCL scaffold production, but rather suggest a methodology to find such parameters when employing new materials. As limitations of the approach proposed here, the need for preliminary trial-and-error sintering tests and the destructive method, i.e. SEM imaging, employed to assess the molten cross-section within

individual struts should be mentioned. However, samples could be non-invasively evaluated by imaging techniques such as micro-computed tomography.

A further limitation of this work is that the scaffolds were tested in the range of elastic deformation only. This did not allow to evaluate their ultimate strength, which is a commonly measured parameter in the characterization of PCL and PCL composite scaffolds produced by SLS (e.g. in [39]). However, the elastic behaviour of the here-investigated scaffold prototypes was regarded most relevant to evaluate the sintering quality in dependency of PCL powders and SLS process parameters. The ultimate strength could be more significantly influenced by the chosen architectural features and local imperfections which were not the primary focus of this work. However, the ultimate strength of the scaffolds should be evaluated prior to implantation *in vivo*.

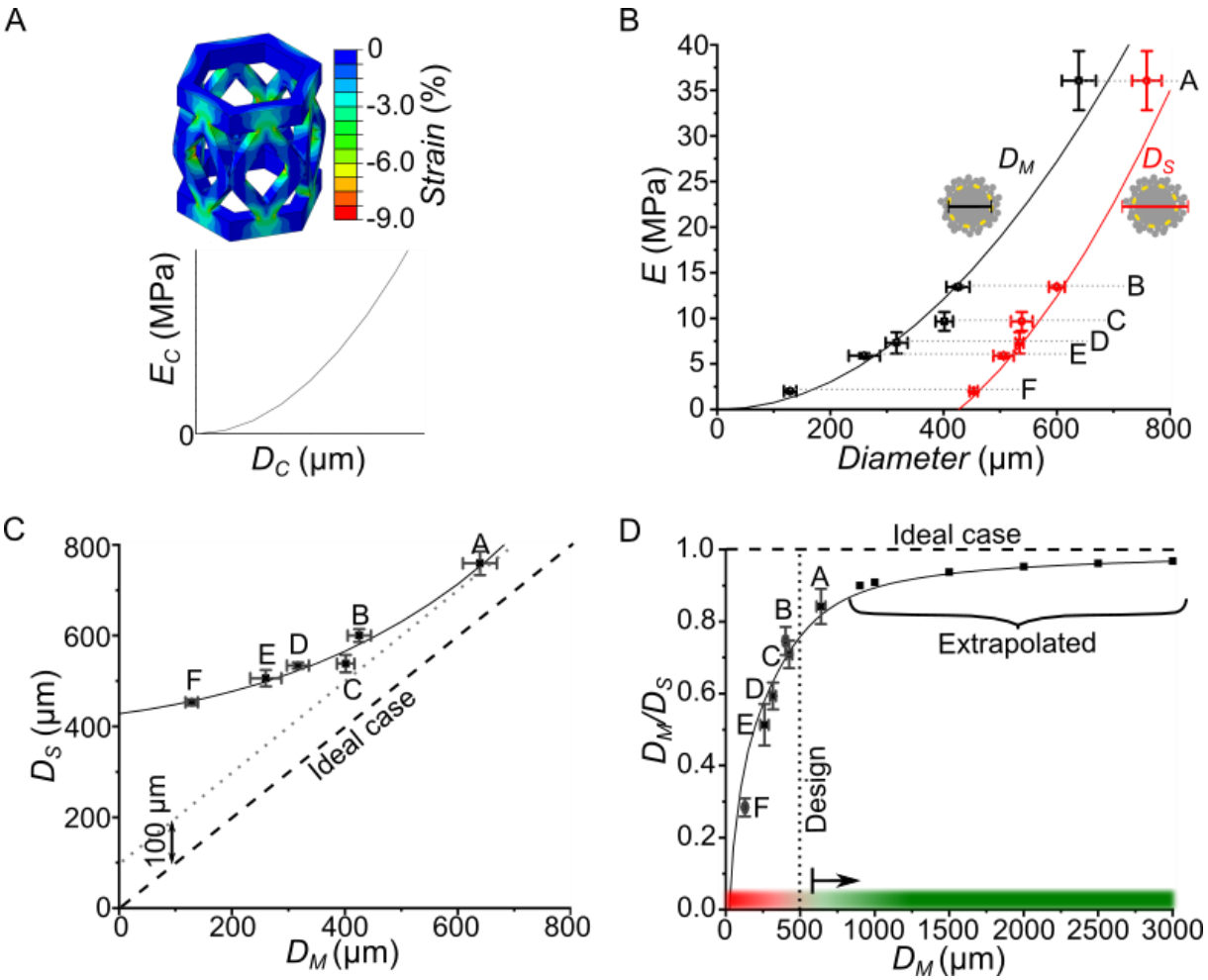

Figure 5: Comparison of prototype properties. A) Top: representative strain distribution in the scaffold as obtained from the FE analysis of the design with D_C = 500 μm. Bottom: in silico-derived relationship between computational elastic modulus (E_C) and computational diameter (D_C); B) experimental elastic modulus (E) as function of molten cross-sectional diameter (D_M, black) and strut diameter (D_S, red). Black and red solid lines represent the polynomial fit of D_M and D_S, respectively; C) D_S as function of D_M. The dashed black line represents the ideal case, i.e. D_S = D_M. The solid black line shows the asymptotic behaviour of the data, where the asymptote is the grey dotted line; D) Ratio D_M/D_S as function of D_M. Six additional points were extrapolated to better show the asymptotic behaviour of the data (solid black line) at large diameters. The black dashed line indicates the D_M/D_S ratio in the ideal case where D_M equals D_S. The black dotted line shows the CAD strut diameter. The colour bar highlights areas of favourable (green) and unfavourable (red) SLS-dependent mechanical stability and the arrow indicates the minimum recommended strut diameter, corresponding to D_M/D_S = 0.8.

3.5 Influence of SLS parameters on scaffold cytocompatibility

Finally, the six prototypes "A" to "F" (see Table 4) were tested for cytocompatibility by evaluating cellular metabolic activity and cell proliferation over 3 and 6 days of *in vitro* culture with human primary mesenchymal stromal cells (hMSCs).

For all tested conditions, cellular metabolic activity increased approximately 2.2- and 4.2-fold at day 3 and 6, respectively, when compared to day 0 (Figure 6A). The rise in metabolic activity could be ascribed to the higher number of cells resulting from cellular proliferation over the 6 days of *in vitro* cell culture (Figure 6B). At day 3, cell number increased approximately 3-fold for all tested conditions. Data points were more scattered at day 6, with a minimum increase of 4.8 ± 0.9-fold and a maximum increase of 5.9 ± 0.9-fold measured for prototypes "D" and "B", respectively, while cell number increased by 4.9 ± 0.9-fold in controls. In summary, no impairment of total cell metabolic activity or cell number was observed when exposing hMSCs to medium conditioned by the investigated prototypes in comparison to unconditioned control. This indicates that, even after processing with SLS with a wide range of process parameters, PCL remains cytocompatible.

The cyto- and biocompatibility of PCL have long been known [6] and the successful *in vitro* culture of various cell phenotypes in PCL scaffolds has been reported for scaffolds produced by SLS [10] and by other production techniques, such as fused deposition modelling [40]. Moreover, the cytocompatibility of the eluate of PCL scaffolds produced by SLS has been previously shown over 3 days of *in vitro* culture with osteoblasts [12], in accordance with the results reported here. To the best of our knowledge, the dependency of the cytocompatibility of PCL scaffolds produced by SLS on the SLS process parameters was not discussed before. Our results indicate that PCL is cytocompatible when the polymer undergoes SLS over a broad range of SLS process parameters.

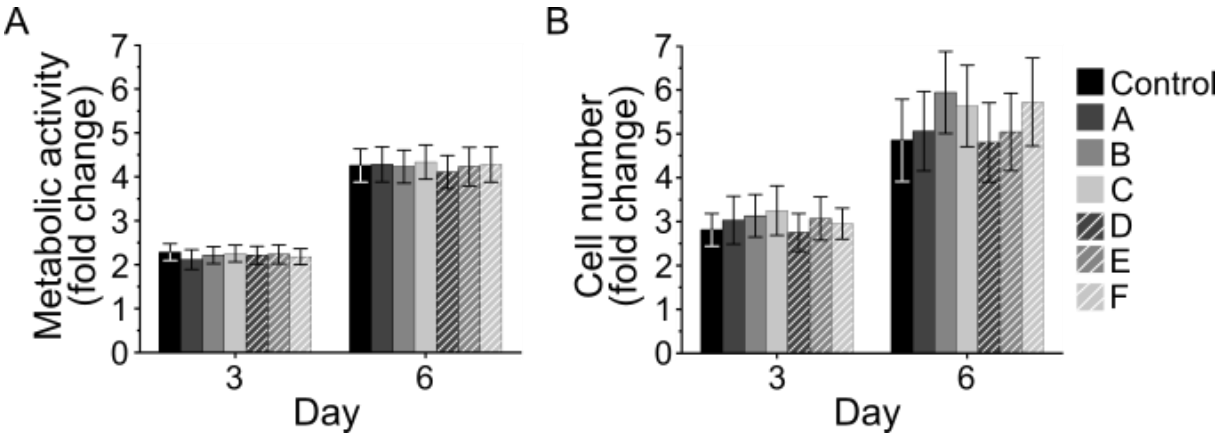

Figure 6: Cytocompatibility of prototypes. A) Cellular metabolic activity; B) Cellular proliferation. Results are normalized to day 0 and given as fold change. The legend to read both plots is on the right side of the figure. Statistical analyses revealed no significant differences in metabolic activity nor in cell number between the control and the six investigated conditions at any time point.

4. Conclusions

Taken together, our data suggest that aiming at dimensional accuracy is not sufficient to determine the ideal SLS parameters for the fabrication of PCL scaffolds for bone TE. We propose to optimize SLS parameters by evaluating both dimensional accuracy and mechanical properties. When considering both factors, we found that multiple sets of SLS parameters were suitable to produce mechanically stable scaffolds. The mechanical stiffness of the scaffold could not be deduced from the outer strut diameter (measured by light microscopy), which is the parameter commonly used for the optimization of process parameters. Rather, the cross-sectional area of fully molten material within the struts (measured by SEM of cryo-cut cross-sections), excluding partially sintered particles, correctly predicted the mechanical stiffness of the scaffolds. Thus, process optimization should aim at maximizing the ratio between molten cross-sectional diameter and strut diameter. This is especially important when producing scaffolds with thin struts, as it is generally the case when a high porosity and a small feature size is required. Dry ice blasting might be used to remove loosely attached particles from the scaffold struts more efficiently compared to air-blasting applied here. In this way, the ratio between molten cross-sectional diameter and strut diameter might be further increased.

We identified a critical minimal value of 590 µm for the diameter of the molten cross-section corresponding to 740 µm outer strut diameter, i.e. including the layer of partially sintered particles, for the specific PCL powder and the SLS machine used here. Below this value, a sufficiently large molten cross-sectional area, and thereby scaffold mechanical stability, could not be guaranteed.

Independently of mechanical properties, prototypes produced with six different sets of SLS process parameters were found to be fully cytocompatible over 6 days of *in vitro* cell culture with primary human mesenchymal stromal cells, confirming the general suitability of SLS as production technique of PCL scaffolds for bone TE.

Acknowledgments

The authors acknowledge funding by the German Federal Ministry of Education and Research (BMBF) via grant numbers 13XP5048D and 13XP5048C. We would like to thank the BIH Center for Regenerative Therapies (BCRT) Core Unit “Cell Harvesting” for providing human mesenchymal stromal cells for this study. Contribution for the PhD student was made possible by DFG funding through the Berlin-Brandenburg School for Regenerative Therapies GSC 203. We thank Prof. Gianluca Ciardelli and Dr. Monica Boffito (Politecnico di Torino) for their support in performing the SEC analysis, Hans Leemhuis (Matricel GmbH) and Andreas Höss (Innotere GmbH) for the helpful discussions and Alessandro Mecconi for reviewing the language.

735 ***Bibliography***

736

737 [1] H.N. Chia, B.M. Wu, Recent advances in 3D printing of biomaterials, J. Biol. Eng. 9
738 (2015) 4. https://doi.org/10.1186/s13036-015-0001-4.

739 [2] R.D. Goodridge, C.J. Tuck, R.J.M. Hague, Laser sintering of polyamides and other
740 polymers, Prog. Mater. Sci. 57 (2012) 229–267.
741 https://doi.org/10.1016/j.pmatsci.2011.04.001.

742 [3] R. Langer, J.P. Vacanti, Tissue Engineering, Science (80-.). 260 (1993) 920–926.
743 https://doi.org/10.1126/science.8493529.

744 [4] B. Thavornyutikarn, N. Chantarapanich, K. Sitthiseripratip, G.A. Thouas, Q. Chen,
745 Bone tissue engineering scaffolding: computer-aided scaffolding techniques, 2014.
746 https://doi.org/10.1007/s40204-014-0026-7.

747 [5] S.F.S. Shirazi, S. Gharehkhani, M. Mehrali, H. Yarmand, H.S.C. Metselaar, N. Adib
748 Kadri, N.A.A. Osman, A review on powder-based additive manufacturing for tissue
749 engineering: selective laser sintering and inkjet 3D printing, Sci. Technol. Adv. Mater.
750 16 (2015) 033502. https://doi.org/10.1088/1468-6996/16/3/033502.

751 [6] M.A. Woodruff, D.W. Hutmacher, The return of a forgotten polymer - Polycaprolactone
752 in the 21st century, Prog. Polym. Sci. 35 (2010) 1217–1256.
753 https://doi.org/10.1016/j.progpolymsci.2010.04.002.

754 [7] J.M. Williams, A. Adewunmi, R.M. Schek, C.L. Flanagan, P.H. Krebsbach, S.E.
755 Feinberg, S.J. Hollister, S. Das, Bone tissue engineering using polycaprolactone
756 scaffolds fabricated via selective laser sintering, Biomaterials. 26 (2005) 4817–4827.
757 https://doi.org/10.1016/j.biomaterials.2004.11.057.

758 [8] A. Mazzoli, C. Ferretti, A. Gigante, E. Salvolini, M. Mattioli-Belmonte, Selective laser
759 sintering manufacturing of polycaprolactone bone scaffolds for applications in bone
760 tissue engineering, Rapid Prototyp. J. 21 (2015) 386–392.
761 https://doi.org/10.1108/RPJ-04-2013-0040.

762 [9] D.A. Zopf, A.G. Mitsak, C.L. Flanagan, M. Wheeler, G.E. Green, S.J. Hollister,
763 Computer aided-designed, 3-dimensionally printed porous tissue bioscaffolds for
764 craniofacial soft tissue reconstruction, Otolaryngol. - Head Neck Surg. (United States).
765 152 (2015) 57–62. https://doi.org/10.1177/0194599814552065.

766 [10] W.Y. Yeong, N. Sudarmadji, H.Y. Yu, C.K. Chua, K.F. Leong, S.S. Venkatraman,
767 Y.C.F. Boey, L.P. Tan, Porous polycaprolactone scaffold for cardiac tissue

768 engineering fabricated by selective laser sintering, Acta Biomater. 6 (2010) 2028–
769 2034. https://doi.org/10.1016/j.actbio.2009.12.033.

770 [11] K.H. Tan, C.K. Chua, K.F. Leong, C.M. Cheah, W.S. Gui, W.S. Tan, F.E. Wiria,
771 Selective laser sintering of biocompatible polymers for applications in tissue
772 engineering, Biomed. Mater. Eng. 15 (2005) 113–124.

773 [12] N. Sudarmadji, J.Y. Tan, K.F. Leong, C.K. Chua, Y.T. Loh, Investigation of the
774 mechanical properties and porosity relationships in selective laser-sintered polyhedral
775 for functionally graded scaffolds, Acta Biomater. 7 (2011) 530–537.
776 https://doi.org/10.1016/j.actbio.2010.09.024.

777 [13] B. Partee, S.J. Hollister, S. Das, Selective Laser Sintering Process Optimization for
778 Layered Manufacturing of CAPA[sup ®] 6501 Polycaprolactone Bone Tissue
779 Engineering Scaffolds, J. Manuf. Sci. Eng. 128 (2006) 531.
780 https://doi.org/10.1115/1.2162589.

781 [14] S. Eshraghi, S. Das, Mechanical & Microstructural Properties of PCL Scaffolds with 1-
782 D, 2-D & 3-D Orthogonally Oriented Porous Architectures Produced by Selective
783 Laser Sintering, Acta Biomater. 6 (2011) 2467–2476.
784 https://doi.org/10.1016/j.actbio.2010.02.002.Mechanical.

785 [15] S. Lohfeld, M.A. Tyndyk, S. Cahill, N. Flaherty, V. Barron, P.E. McHugh, A method to
786 fabricate small features on scaffolds for tissue engineering via selective laser sintering,
787 J. Biomed. Sci. Eng. 03 (2010) 138–147. https://doi.org/10.4236/jbise.2010.32019.

788 [16] K.F. Leong, C.K. Chua, W.S. Gui, Verani, Building porous biopolymeric
789 microstructures for controlled drug delivery devices using selective laser sintering, Int.
790 J. Adv. Manuf. Technol. 31 (2006) 483–489. https://doi.org/10.1007/s00170-005-0217-
791 4.

792 [17] S. Bose, M. Roy, A. Bandyopadhyay, Recent advances in bone tissue engineering
793 scaffolds, Trends Biotechnol. 30 (2012) 546–554.
794 https://doi.org/10.1016/j.tibtech.2012.07.005.

795 [18] R. Florencio-Silva, G. Rodriguez da Silva Sasso, E. Sasso-Cerri, M.J. Simoes, P.S.
796 Cerri, Biology of Bone Tissue: Structure, Function, and Factors That Influence Bone
797 Cells, Biomed Res. Int. (2015). https://doi.org/10.1016/S0923-2532(05)80182-6.

798 [19] M. Boffito, C. Pontremoli, S. Fiorilli, R. Laurano, G. Ciardelli, C. Vitale-Brovarone,
799 Injectable thermosensitive formulation based on polyurethane hydrogel/mesoporous
800 glasses for sustained co-delivery of functional ions and drugs, Pharmaceutics. 11

(2019). https://doi.org/10.3390/pharmaceutics11100501.

[20] R. Nunes, J. Martin, J. Johnson, Influence of molecular weight and molecular weight distribution on mechanical properties of polymers, Polym. Eng. Sci. 22 (1982) 205–228. https://doi.org/10.1002/pen.760220402.

[21] A. D'Olubamiji, Z. Izadifar, J.L. Si, D.M.L. Cooper, F. Eames, D.X.B. Chen, Modulating mechanical behaviour of 3D-printed cartilage-mimetic PCL scaffolds : influence of molecular weight and pore geometry, Biofabrication. (2016).

[22] M. Grosvenor, J. Staniforth, The effect of molecular weight on the rheological and tensile properties of poly (ϵ-caprolactone), Int. J. Pharm. 135 (1996) 103–109.

[23] C.T. Bellehumeur, M.K. Bisaria, J. Vlachopoulos, An experimental study and model assessment of polymer sintering, Polym. Eng. Sci. 36 (1996) 2198–2207. https://doi.org/10.1002/pen.10617.

[24] C. Gayer, J. Ritter, M. Bullemer, S. Grom, L. Jauer, W. Meiners, A. Pfister, F. Reinauer, M. Vučak, K. Wissenbach, H. Fischer, R. Poprawe, J.H. Schleifenbaum, Development of a solvent-free polylactide/calcium carbonate composite for selective laser sintering of bone tissue engineering scaffolds, Mater. Sci. Eng. C. 101 (2019) 660–673. https://doi.org/10.1016/j.msec.2019.03.101.

[25] F. Tuba, L. Oláh, P. Nagy, Towards the understanding of the molecular weight dependence of essential work of fracture in semi-crystalline polymers: A study on poly(ε-caprolactone), Express Polym. Lett. 8 (2014) 869–879. https://doi.org/10.3144/expresspolymlett.2014.88.

[26] J.K. Prescott, R.A. Barnum, On powder flowability, Pharm. Technol. 24 (2000) 60-84+236.

[27] B. Trathnigg, Size-Exclusion Chromatography of Polymers, in: R.A. Meyers (Ed.), Encycl. Anal. Chem., John Wiley & Sons, Ltd, Chichester, UK, 2006: pp. 8008–8034. https://doi.org/10.1002/9780470027318.a2032.

[28] L.A. Bosworth, A. Gibb, S. Downes, Gamma irradiation of electrospun poly(ε-caprolactone) fibers affects material properties but not cell response, J. Polym. Sci. Part B Polym. Phys. 50 (2012) 870–876. https://doi.org/10.1002/polb.23072.

[29] E. Cottam, D.W.L. Hukins, K. Lee, C. Hewitt, M.J. Jenkins, Effect of sterilisation by gamma irradiation on the ability of polycaprolactone (PCL) to act as a scaffold material, Med. Eng. Phys. 31 (2009) 221–226. https://doi.org/10.1016/j.medengphy.2008.07.005.

[30] R. Augustine, A. Saha, V.P. Jayachandran, S. Thomas, N. Kalarikkal, Dose-dependent effects of gamma irradiation on the materials properties and cell proliferation of electrospun polycaprolactone tissue engineering scaffolds, Int. J. Polym. Mater. Polym. Biomater. 64 (2015) 526–533. https://doi.org/10.1080/00914037.2014.977900.

[31] D.S. Jones, J. Djokic, C.P. McCoy, S.P. Gorman, Poly(ε-caprolactone) and poly(ε-caprolactone)-polyvinylpyrrolidone-iodine blends as ureteral biomaterials: Characterisation of mechanical and surface properties, degradation and resistance to encrustation in vitro, Biomaterials. 23 (2002) 4449–4458. https://doi.org/10.1016/S0142-9612(02)00158-8.

[32] H. Sun, L. Mei, C. Song, X. Cui, P. Wang, The in vivo degradation, absorption and excretion of PCL-based implant, Biomaterials. 27 (2006) 1735–1740. https://doi.org/10.1016/j.biomaterials.2005.09.019.

[33] S.C. Woodward, P.S. Brewer, F. Moatamed, A. Schindler, C.G. Pitt, The intracellular degradation of poly(ε-caprolactone), J. Biomed. Mater. Res. 19 (1985) 437–444. https://doi.org/10.1002/jbm.820190408.

[34] O. Gil-Castell, J.D. Badia, E. Strömberg, S. Karlsson, A. Ribes-Greus, Effect of the dissolution time into an acid hydrolytic solvent to taylor electrospun nanofibrous polycaprolactone scaffolds, Eur. Polym. J. 87 (2017) 174–187. https://doi.org/10.1016/j.eurpolymj.2016.12.005.

[35] V.S. Sukanya, P. V. Mohanan, Degradation of Poly(ε-caprolactone) and bio-interactions with mouse bone marrow mesenchymal stem cells, Colloids Surfaces B Biointerfaces. 163 (2018) 107–118. https://doi.org/10.1016/j.colsurfb.2017.12.039.

[36] D.L. Bourell, T.J. Watt, D.K. Leigh, B. Fulcher, Performance limitations in polymer laser sintering, Phys. Procedia. 56 (2014) 147–156. https://doi.org/10.1016/j.phpro.2014.08.157.

[37] B.E. Franco, J. Ma, B. Loveall, G.A. Tapia, K. Karayagiz, J. Liu, A. Elwany, R. Arroyave, I. Karaman, A Sensory Material Approach for Reducing Variability in Additively Manufactured Metal Parts, Sci. Rep. 7 (2017) 1–12. https://doi.org/10.1038/s41598-017-03499-x.

[38] R. Vrána, O. Cervinek, P. Manas, D. Koutný, D. Paloušek, Dynamic loading of lattice structure made by selective laser melting-numerical model with substitution of geometrical imperfections, Materials (Basel). 11 (2018). https://doi.org/10.3390/ma11112129.

[39] C. Shuai, L. Yu, P. Feng, Y. Zhong, Z. Zhao, Z. Chen, W. Yang, Organic montmorillonite produced an interlayer locking effect in a polymer scaffold to enhance interfacial bonding, Mater. Chem. Front. 4 (2020) 2398–2408. https://doi.org/10.1039/d0qm00254b.

[40] D.W. Hutmacher, J.T. Schantz, I. Zein, K.W. Ng, S.H. Teoh, K.C. Tan, Mechanical properties and cell cultural response of polycaprolactone scaffolds designed and fabricated via fused deposition modeling, J. Biomed. Mater. Res. 55 (2001) 203–216. https://doi.org/10.1002/1097-4636(200105)55:2<203::AID-JBM1007>3.0.CO;2-7.